Figure S1

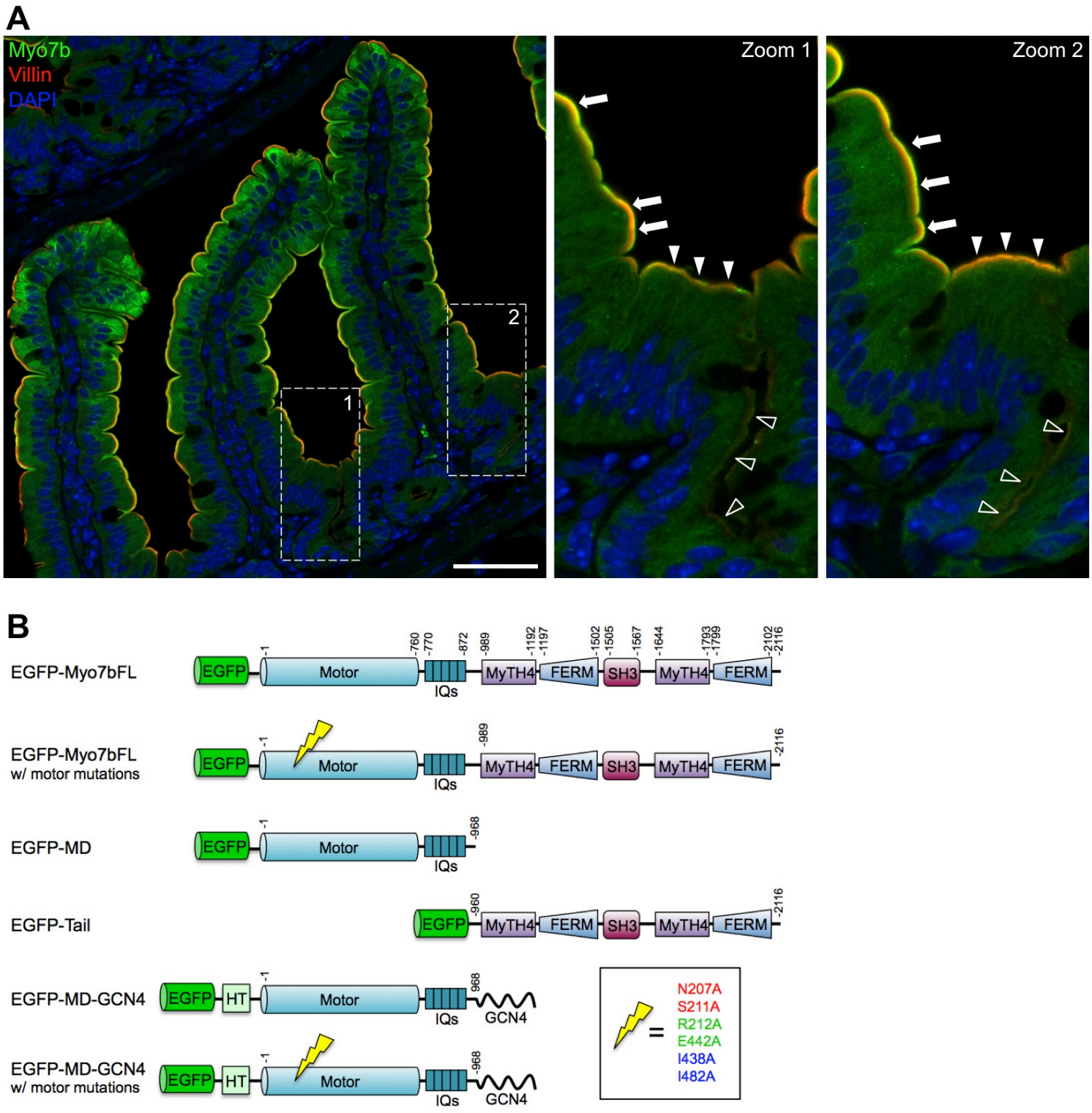
A
Myo7b
Villin
DAPI
1
2
Zoom 1
Zoom 2
B
EGFP-Myo7bFL
EGFP-Myo7bFL
w/ motor mutations
EGFP-MD
EGFP-Tail
EGFP-MD-GCN4
EGFP-MD-GCN4
w/ motor mutations
EGFP
HT
Motor
IQs
MyTH4
FERM
SH3
GCN4
-1
-760
-770
-872
-989
-1192
-1197
-1502
-1505
-1567
-1644
-1793
-1799
-2102
-2116
-968
-960
N207A
S211A
R212A
E442A
I438A
I482A

Figure S2

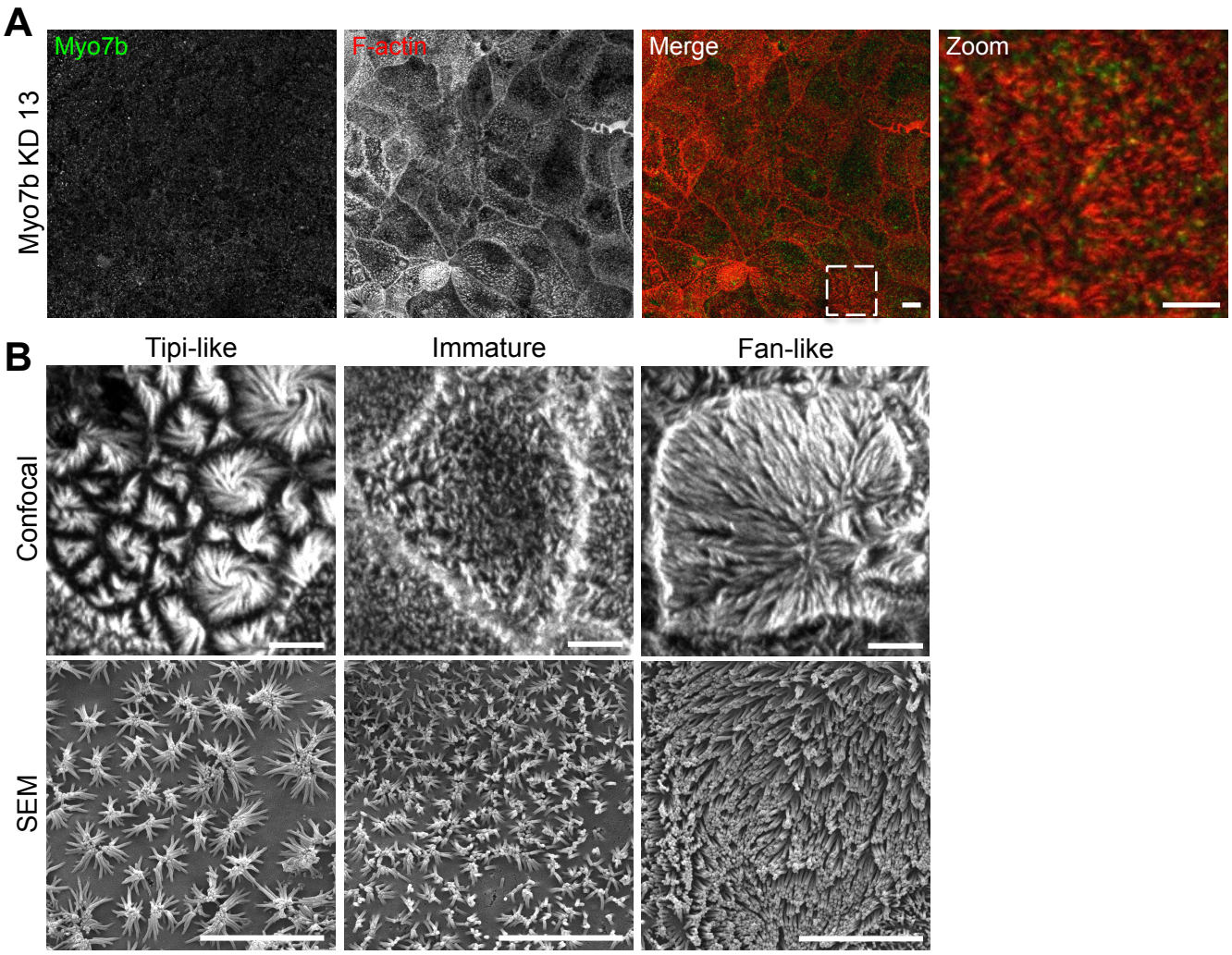
A
Myo7b KD 13
Myo7b
F-actin
Merge
Zoom
B
Tipi-like
Immature
Fan-like
Confocal
SEM

Figure S3

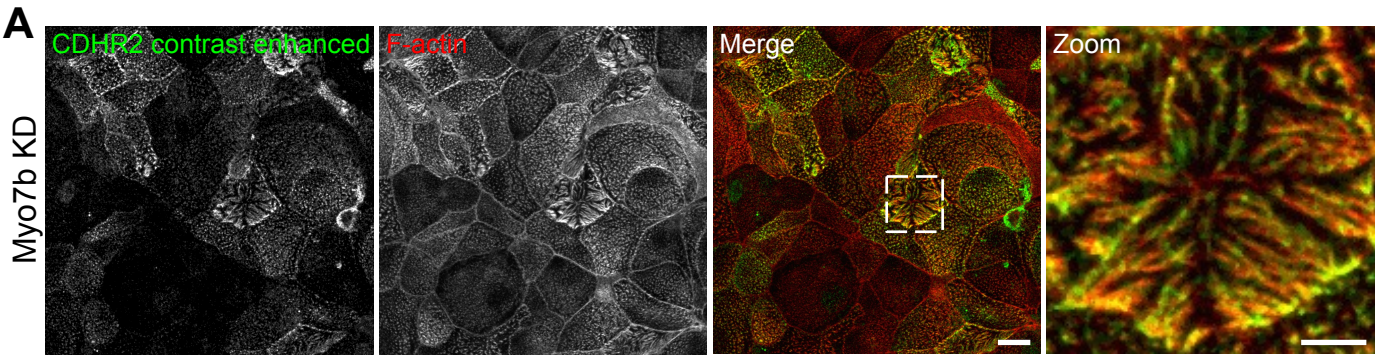
A
Myo7b KD
CDHR2 contrast enhanced
F-actin
Merge
Zoom

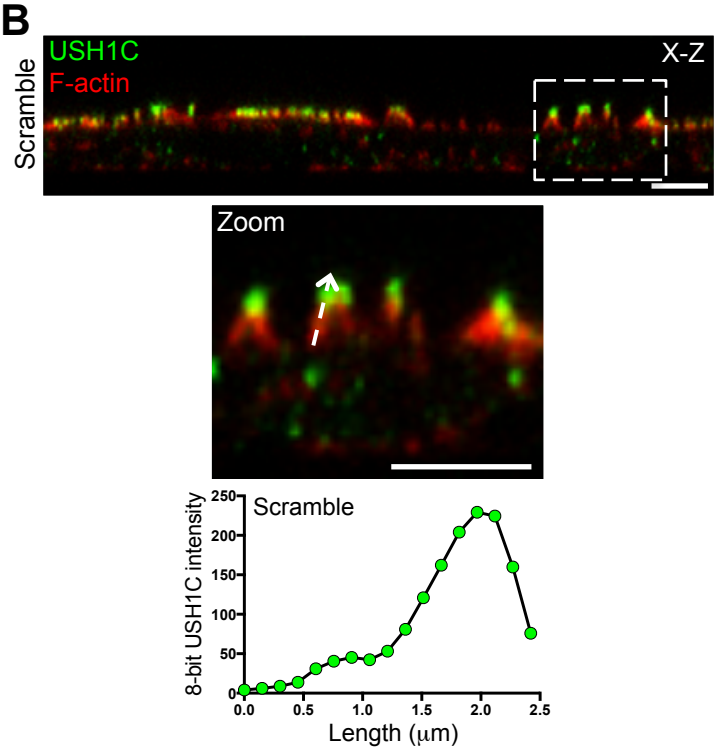
B
Scramble
USH1C
F-actin
X-Z
Zoom
Scramble
8-bit USH1C intensity
Length (μm)
Normalize length to 0=base and 1=tip
Combine multiple line scans
Normalize pooled data sets to 0=lowest intensity and 1=high intensity
Plot and fit to single or double Gaussian

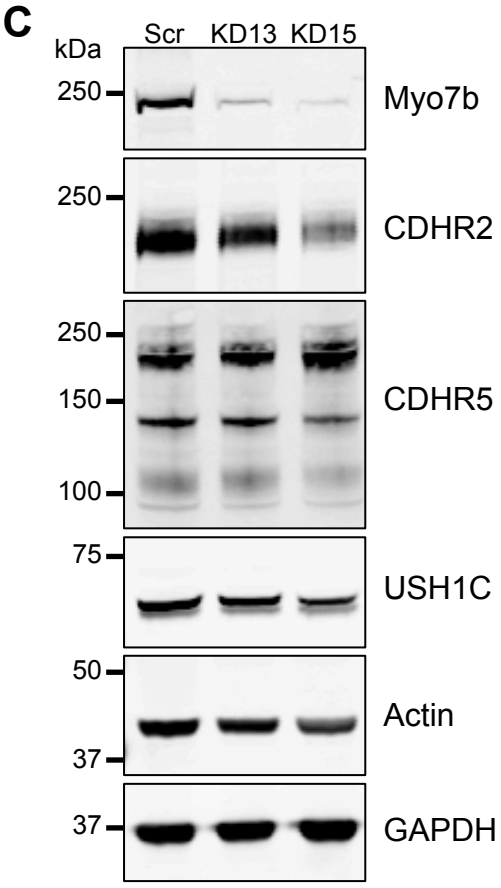
C
kDa
Scr
KD13
KD15
Myo7b
CDHR2
CDHR5
USH1C
Actin
GAPDH

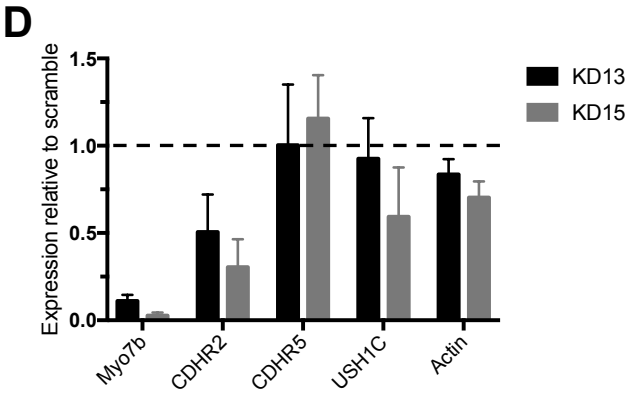
D
Expression relative to scramble
KD13
KD15
Myo7b
CDHR2
CDHR5
USH1C
Actin

A

Dd Myo2	*Hs* Myo7b	Actin movement	Actin binding	ATPase activity
N233A	N207A	None	Strong	None
S237A	S211A	None	Strong	None
R238A	R212A	None	Weak	None
E459A	E442A	None	Weak	None
I455M	I438A	None	WT	WT
I499A	I482A	None	WT	WT

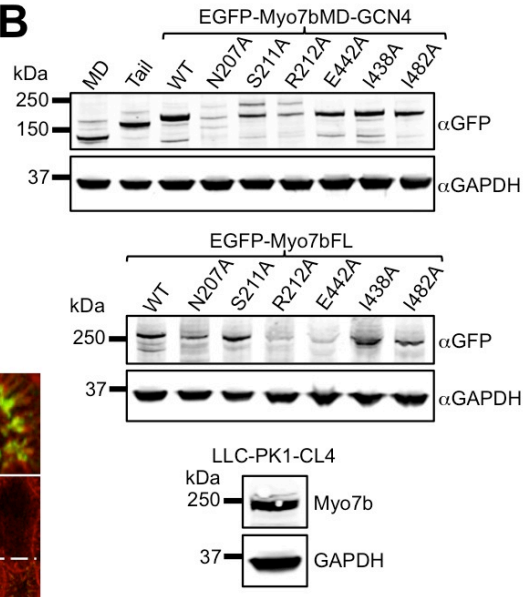

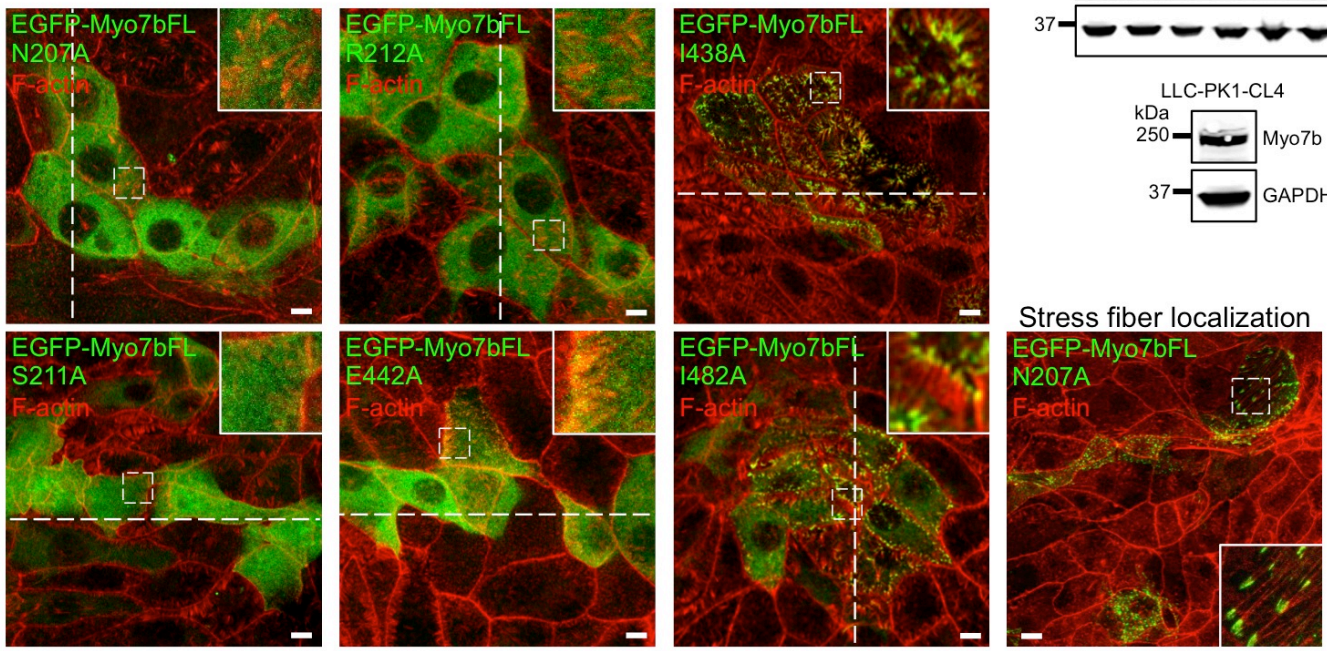

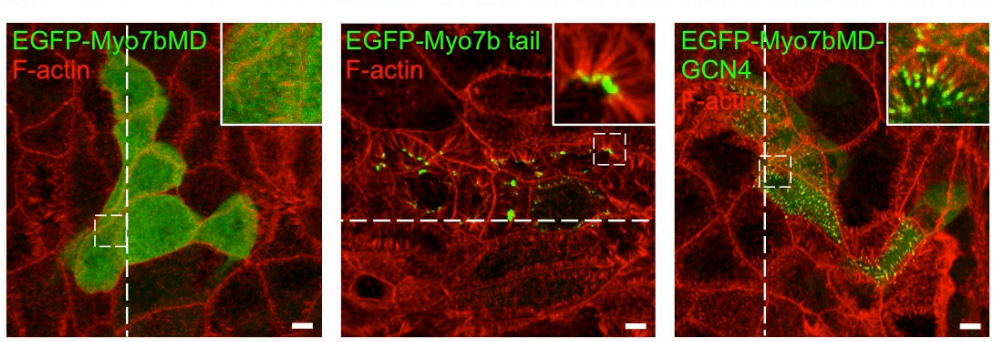

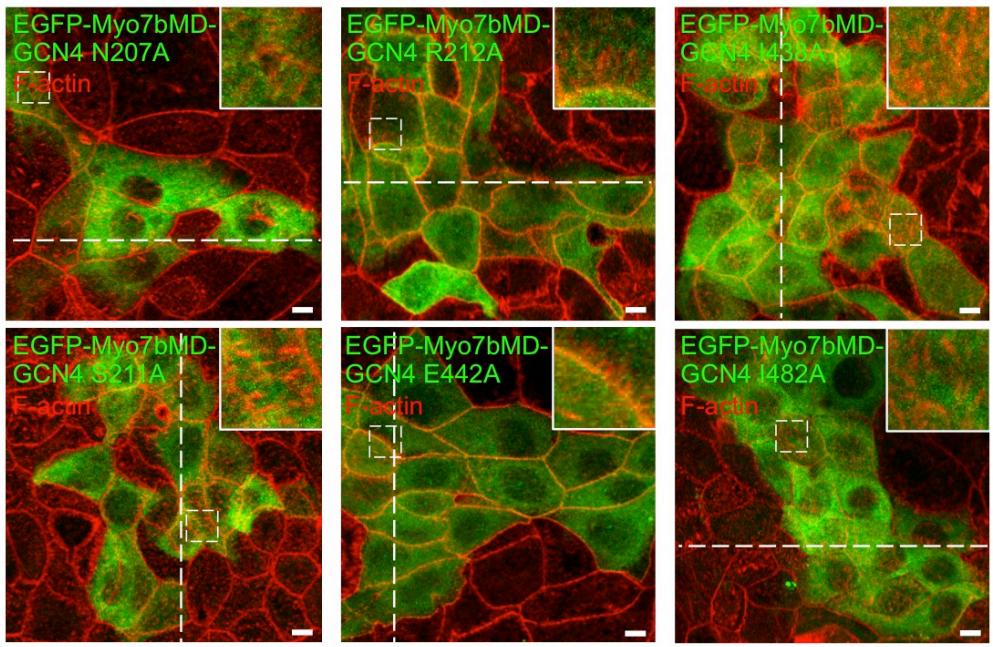

Figure S4

Figure S5

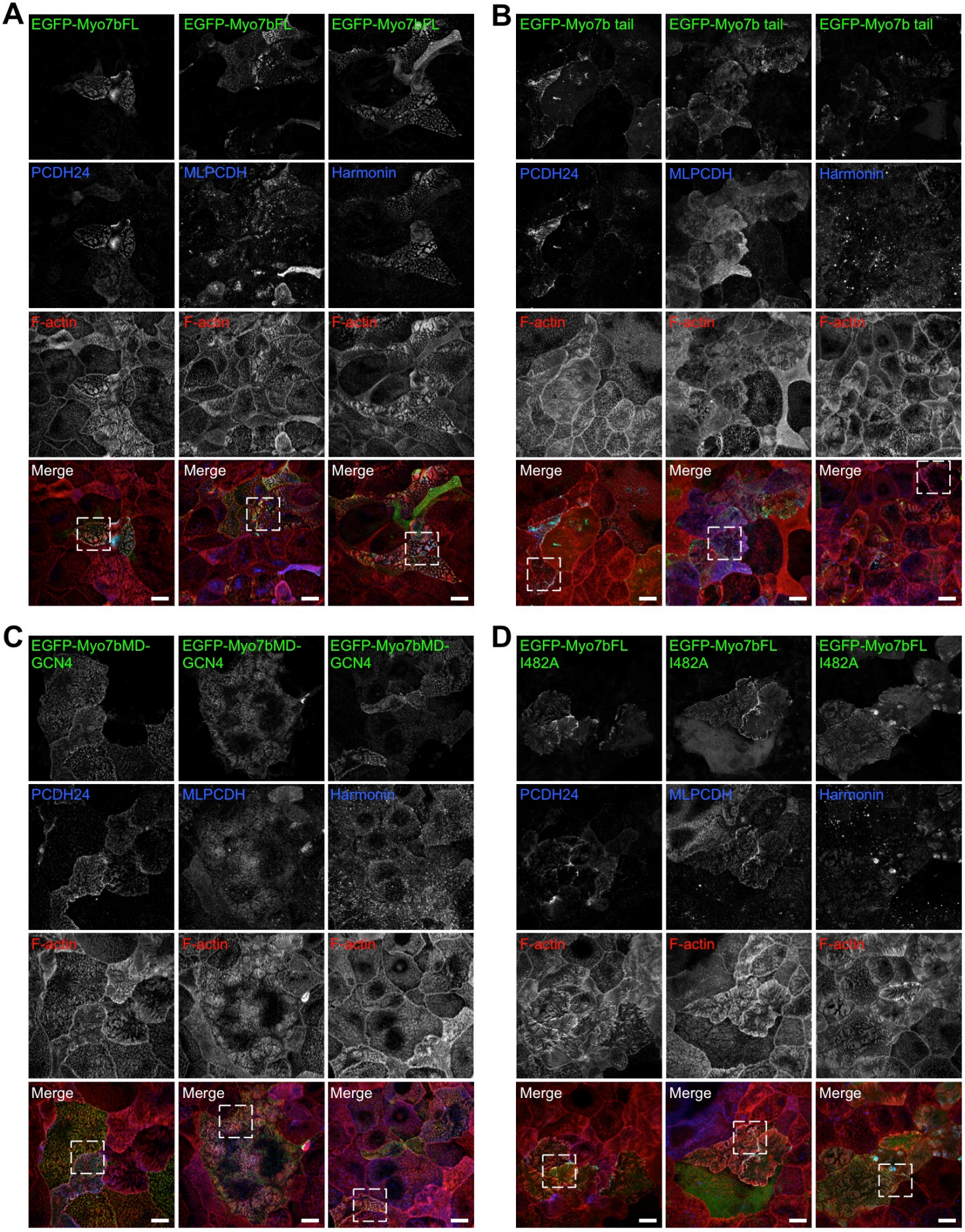
A
EGFP-Myo7bFL
EGFP-Myo7bFL
EGFP-Myo7bFL
PCDH24
MLPCDH
Harmonin
F-actin
F-actin
F-actin
Merge
Merge
Merge
B
EGFP-Myo7b tail
EGFP-Myo7b tail
EGFP-Myo7b tail
PCDH24
MLPCDH
Harmonin
F-actin
F-actin
F-actin
Merge
Merge
Merge
C
EGFP-Myo7bMD-GCN4
EGFP-Myo7bMD-GCN4
EGFP-Myo7bMD-GCN4
PCDH24
MLPCDH
Harmonin
F-actin
F-actin
F-actin
Merge
Merge
Merge
D
EGFP-Myo7bFL I482A
EGFP-Myo7bFL I482A
EGFP-Myo7bFL I482A
PCDH24
MLPCDH
Harmonin
F-actin
F-actin
F-actin
Merge
Merge
Merge

SUPPLEMENTAL FIGURE LEGENDS

Figure S1, related to Figure 1. Myo7b localization along the crypt-villus axis in native tissue.
(A) Confocal images of mouse intestinal tissue stained for Myo7b (green), villin (red), and DAPI (blue). Boxed areas indicate regions in zoomed images. Open arrowheads point to crypt microvilli with little expression of Myo7b and villin. Filled arrowheads point to the crypt-villus transition where Myo7b and villin expression begins to increase. Arrows point to robust distal tip enrichment of Myo7b within the brush border on the villus. Scale bar, 50 μm. (B) Constructs of Myo7b used in this study. Numbers indicate amino acids; HaloTag (HT).

Figure S2, related to Figure 2. Loss of Myo7b in CACO-2_{BBE} cells decreases microvillar clustering.
(A) Confocal images of Myo7b (green) and F-actin (red) of Myo7b KD13 CACO-2_{BBE} cells at 14 DPC. Boxed area indicates region in zoomed image. Scale bars, 10 μm; 5 μm in zoom. (B) Confocal images of F-actin (top row) and SEM images (bottom row) of the different BB morphologies observed in CACO-2_{BBE} cells. Only cells with tipi-like clusters were counted as cells with clustering microvilli in quantifications. Scale bars, 5 μm.

Figure S3, related to Figure 3. Myo7b KD in CACO-2_{BBE} cells results in a decrease of IMAC expression.
(A) Confocal images from Figure 3A that have been contrast enhanced to show the decreased expression and localization of CDHR2 (green) along the microvillar axis, F-actin (red), in Myo7b KD cells at 14 DPC. Boxed area indicates region in zoomed image. Scale bars, 10 μm; 5 μm in zoom. (B) Illustration of how line scans were acquired, combined, and normalized. Vertical section from confocal image of USH1C (green) and F-actin (red) of scramble CACO-2_{BBE} cells at 14 DPC. Boxed area indicates region in zoomed image. Dashed arrow indicates line scan used to generate plot. Scale bars, 5 μm. (C) Western blot analysis of endogenous CDHR2, CDHR5, USH1C, and actin in lysates from 14 DPC scramble control and two independent Myo7b KD stable cell lines. (D) Quantification of endogenous Myo7b, CDHR2, CDHR5, USH1C, and actin in lysates from 14 DPC scramble control and two independent Myo7b KD stable cell lines. Values are expressed relative to scramble.

Figure S4, related to Figure 4. Structure-function analysis of Myo7b motor requirements for tip targeting
(A) Motor domain point mutations generated in human (*Hs*) Myo7b compared to the mutational analyses done previously in *Dictyostelium discoideum* (*Dd*) myosin 2 [S1-4]. (B) Western blot analysis of construct expression in LLC-PK1-CL4 stable cell lines at 4 DPC and endogenous Myo7b from wild-type LLC-PK1-CL4 cells at 4 DPC. (C) Confocal images of motor domain mutations in the full-length Myo7b construct. Boxed areas indicate regions in zoomed insets. Dashed lines indicate X-Z vertical sections shown in Figure 4. Scale bars, 5 μm; 10 μm in stress fiber localization image. (D) Confocal images of deletion and forced dimer constructs of Myo7b. Boxed areas indicate regions in zoomed insets. Dashed lines indicate X-Z vertical sections shown in Figure 4. Scale bars, 5 μm. (E) Confocal images of motor domain mutations in the forced dimer Myo7b construct. Boxed areas indicate regions in zoomed insets. Dashed lines indicate X-Z vertical sections shown in Figure 4. Scale bars, 5 μm.

Figure S5, related to Figure 5. Rescue of Myo7b KD phenotypes in CACO-2_{BBE} cells with refractory constructs.
Lower magnification single channel and merge versions of confocal images presented in Figure 5A. (A) EGFP-Myo7bFL, (B) EGFP-Myo7b tail, (C) EGFP-Myo7bMD-GCN4, and (D) EGFP-Myo7bFL I482A. Boxed areas indicate regions in zoomed images shown in Figure 5A. Scale bars, 15 μm.

SUPPLEMENTAL EXPERIMENTAL PROCEDURES

Cloning and constructs

The human cDNA construct of Myo7b used in this study was GI: 122937511. Full-length (amino acids [aa] 1-2116), MD (aa 1-968), and tail (aa 960-2116) constructs were generated by PCR and TOPO cloned into the pCR8 Gateway entry vector (Invitrogen). The forced dimer (MD-GCN4) construct was created by introducing the GCN4 leucine zipper sequence after L968 using 5' ScaI and 3' HindIII sites. The subsequent amino acid sequence immediately follows L968: STMKQLEDKVEELLSKNYHLENEVARLKKLVGE. Restriction enzyme sites, point mutations, and refractory silent mutations were introduced using QuikChange site-directed mutagenesis (Agilent). All entry vectors were verified by DNA sequencing. The entry vectors were then shuttled into destination vectors pEGFP-C1 (Clontech) and pINDUCER20-EGFP-C1 [S5] that were Gateway-adapted using the Gateway vector conversion kit (Invitrogen). A non-targeting scramble control shRNA (Addgene; plasmid 1864) and Myo7b KD shRNA clones were expressed in pLKO.1, corresponding to TRC clones TRCN0000247713 and TRCN0000247715 (Sigma).

Transient transfections and lentivirus production

For transient transfections of Cos-7 cells, transfections were performed using Lipofectamine 2000 (Invitrogen) according to the manufacturer's instructions and the cells were allowed to recover ON. The following day, cells were plated on glass-bottom dishes coated with 25 mg/ml laminin (Sigma), and allowed to adhere for two hours before imaging. Lentiviral particles were generated by cotransfecting HEK293FT cells with overexpression (pINDUCER20-EGFP-C1) or KD (pLKO.1) plasmids along with the packaging psPAX2 and envelope pMD2.G plasmids using FuGENE 6 (Promega). Cells were incubated for 2 days to allow for lentivirus production before collecting the media containing lentiviral particles. Media was centrifuged at 500xg for 10 mins at 4°C to remove cells and concentrated using Lenti-X Concentrator (Clontech).

Western blot analysis of CACO-2_{BBE} KD cell lines and LLC-PK1-CL4 stable cell lines

CACO-2_{BBE} and LLC-PK1-CL4 stable cell lines were seeded into T25 flasks and grown until 14 DPC or 4 DPC, respectively. Cells were washed once with warm PBS and recovered in 5 mL of PBS using a cell scraper. Cells were pelleted at low speed and resuspended in RIPA buffer containing 1mM ATP, 1mM Pefabloc SC (Roche), and 1x cOmplete ULTRA protease inhibitor cocktail (Roche). Cells were lysed by needle aspiration and centrifuged at 16,000xg for 5 min at 4°C. The soluble fraction was recovered and SDS sample buffer was added to a 2x final concentration before being boiled for 3 min. Samples were then separated on 4-12% NuPAGE Bis-Tris gel (Novex) and transferred in Towbin buffer, pH 8.3, to nitrocellulose at 15 V ON. Membranes were blocked for 1 hr in 5% milk in PBS containing 0.1% Tween-20 (PBS-T), washed once with PBS-T, and then incubated with primary antibodies against Myo7b (1:100; Sigma cat. #HPA039131), CDHR2 (1:100; Sigma cat. #HPA012569), CDHR5 (1:500; Sigma cat. #HPA009081), USH1C (1:250; Sigma cat. #HPA027398), GAPDH (1:1000; Cell Signaling cat. #2118L), actin (1:1000; Sigma cat. #A2066), or anti-GFP (1:1,000; Aves labs Cat#GFP1020) in 5% milk PBS-T for 2 hrs. Membranes were washed three times with PBS-T and incubated with goat anti-rabbit 800 IRdye (1:10,000; Li-Cor) or donkey anti-chicken 800 IRdye (1:10,000; Li-Cor) in 5% milk PBS-T for 1 hr. Membranes were washed four times with PBS-T before being imaged using a Li-Cor Odyssey infrared imaging system. Images of membrane scans were contrast enhanced and quantified using ImageJ (NIH) with the signal from GAPDH used to normalize sample loading.

Light microscopy

CACO-2_{BBE} cells were washed once with warm PBS and fixed with 4% paraformaldehyde in PBS for 15 min at 37°C. After fixation, cells were washed three times with PBS and permeabilized with 0.1% Triton X-100 in PBS for 15 min at room temperature (RT). Cells were then washed three times with

PBS and blocked ON with 5% BSA in PBS at 4°C. Cells were washed once with PBS and immunostaining was performed using anti-PCDH24 (1:75; Sigma cat#HPA012569), anti-MLPCDH (1:250; Sigma cat#HPA009081), anti-harmonin (1:70; Sigma cat#HPA027398), and anti-Myo7b (1:25; Sigma cat#HPA039131) at RT for 2 hours. Coverslips were then washed three times with PBS and incubated with Alexa Fluor 488 goat anti-rabbit or Alexa Fluor 647 goat anti-rabbit and Alexa Fluor 568 phalloidin (1:200; Life Technologies) diluted 1:200 in PBS for 1 hour at 37°C. Cells were washed four times with PBS and coverslips were mounted using ProLong Gold Antifade Mountant (Life Technologies). LLC-PK1-CL4 cells were washed once with warm PHEM buffer (60 mM PIPES, 25 mM HEPES, 5 mM EGTA, 3% sucrose, pH 7.0) and briefly live cell extracted with warm 0.02% saponin in PHEM buffer. Following extraction, cells were fixed with 4% paraformaldehyde in PHEM buffer containing 0.1% Triton X-100 at 37°C for 10 min. Cells were then washed three times with PBS and stained with Alexa Fluor 568 phalloidin (1:200) in PBS for 30 min at 37°C. Coverslips were washed and mounted as above. For super-resolution microscopy, cells were live cell extracted as above. After fixation, cells were washed three times with PBS and blocked ON with 5% BSA in PBS at 4°C. Cells were washed once with PBS and stained with anti-GFP (1:200; Aves labs Cat#GFP1020) for 2 hours at RT. Coverslips were then washed three times with PBS and incubated with Alexa Fluor 488 goat anti-chicken and Alexa Fluor 568 phalloidin (1:200; Life Technologies) diluted 1:200 in PBS for 1 hour at 37°C. Cells were washed four times with PBS and coverslips were mounted using ProLong Gold Antifade Mountant. For TIRF live cell imaging, cells were maintained in a humid environment at RT and 5% CO2 using a stage-top incubation system (Tokai Hit). Image acquisition was controlled with Nikon Elements software.

Immunohistofluorescence

Paraffin-embedded tissues sections of wild-type mouse kidney and small intestinal Swiss roles were deparaffinized using Histo-clear solution (Fisher) and rehydrated in a descending graded ethanol series. The sample slides were then subjected to an antigen retrieval step, consisting of boiling for 1 hr in a solution of 10 mM Tris (pH 9.0) and 0.5 mM EGTA. Samples were washed three times with PBS and blocked ON at 4°C in 10% goat serum in PBS. Slides were then washed in PBS three times and stained ON at 4°C with anti-Myo7b (1:25; Sigma cat#HPA039131) and anti-villin (1:50; Santa Cruz cat. #sc58897) in 1% goat serum in PBS. After washing with PBS four times, samples were stained with Alexa Fluor 488 F(ab')2 goat anti-rabbit and Alexa Fluor 568 F(ab')2 goat anti-mouse (1:1,000; Life Technologies) in 1% goat serum in PBS for 1 hr at RT. Slides were then washed four times with PBS, dehydrated in an ascending graded ethanol series, and mounted in ProLong Gold Antifade Mountant with or without DAPI.

Electron microscopy

All SEM reagents were purchased from Electron Microscopy Sciences. CACO-2_{BBE} cells were seeded at a density of 200,000 cells/well into 0.4-mm 12-mm Transwell-COL inserts (Corning) and allowed to grow to 8 or 20 DPC. Samples were washed once with warm PBS and fixed overnight at 4°C with 3% glutaraldehyde in SEM buffer (0.1 M sucrose and 0.1 M Na-phosphate, pH 7.4). Samples were washed with SEM buffer, postfixed with 1% OsO_4 in SEM buffer on ice for 1 h, and washed with SEM buffer. Samples were dehydrated in a graded ethanol series, dried with hexamethyldisilazane, mounted on aluminum stubs, coated with gold/platinum in a sputter coater.

Image analysis

All image analysis was done using ImageJ. Using the phalloidin signal, line scan analyses of tip enrichment were done by drawing lines parallel to the microvillar axis, starting at the base of the microvillus and extending to the end of the tip. For confocal stacks, measurements were taken using X-Z and Y-Z vertical sections. Intensities of Myo7b or CDHR2 along the line were taken and normalized from 0 to 1, with 0 representing the lowest intensity measurement and 1 representing the highest. Microvillar length for each line was also normalized from 0 to 1, with 0 representing the base

and 1 representing the tip. Normalized line scans were then plotted together and fitted to either a sum of two (Figure 1) or single Gaussian (Figure 3 and 5) using non-linear regression (Prism v.7, GraphPad). The resulting fit revealed the position of peak intensity and distribution width (SD) relative to the microvillar axis. Line scan analysis of microvillar clustering was done by drawing lines along the long axis of five cells in inverted phalloidin images. 8-bit intensities of the phalloidin signal were plotted and stacked onto one graph. Individual cells were scored for microvillar clustering as described previously [S6]. Microvillar tip targeting measurements were taken by using X-Z and Y-Z vertical sections from confocal stacks. The intensity at the tip of an individual microvillus was divided by the cytoplasmic intensity underneath that microvillus. For each cell, 5 microvillar tip to cyplasmic ratios were averaged, and then binned into a category based on the averaged ratio: no targeting (ratio of <1), moderate targeting (ratio of 1-2.5), and robust targeting (ratio of >2.5). Results were graphed as a percentage of the total number of cells each category occupied. For each stable cell line, at least 20 cells were quantified. CDHR2 intensities were measured by outlining each EGFP-positive cell and recording the mean 8-bit intensity of the far-red channel.

Animal Studies

Animal experiments were carried out in accordance with Vanderbilt University Medical Center Institutional Animal Care and Use Committee guidelines.

References

S1. Shimada, T., Sasaki, N., Ohkura, R., and Sutoh, K. (1997). Alanine scanning mutagenesis of the switch I region in the ATPase site of Dictyostelium discoideum myosin II. Biochemistry *36*, 14037-14043.

S2. Sasaki, N., Shimada, T., and Sutoh, K. (1998). Mutational analysis of the switch II loop of Dictyostelium myosin II. The Journal of biological chemistry *273*, 20334-20340.

S3. Kambara, T., Rhodes, T.E., Ikebe, R., Yamada, M., White, H.D., and Ikebe, M. (1999). Functional significance of the conserved residues in the flexible hinge region of the myosin motor domain. The Journal of biological chemistry *274*, 16400-16406.

S4. Sasaki, N., Ohkura, R., and Sutoh, K. (2003). Dictyostelium myosin II mutations that uncouple the converter swing and ATP hydrolysis cycle. Biochemistry *42*, 90-95.

S5. Crawley, S.W., Weck, M.L., Grega-Larson, N.E., Shifrin, D.A., Jr., and Tyska, M.J. (2016). ANKS4B Is Essential for Intermicrovillar Adhesion Complex Formation. Developmental cell *36*, 190-200.

S6. Crawley, S.W., Shifrin, D.A., Jr., Grega-Larson, N.E., McConnell, R.E., Benesh, A.E., Mao, S., Zheng, Y., Zheng, Q.Y., Nam, K.T., Millis, B.A., et al. (2014). Intestinal brush border assembly driven by protocadherin-based intermicrovillar adhesion. Cell *157*, 433-446.